Monthly Notices
of the
ROYAL ASTRONOMICAL SOCIETY

MNRAS **437,** 2361–2375 (2014)
Advance Access publication 2013 November 28

doi:10.1093/mnras/stt2054

Gemini multiconjugate adaptive optics system review – I. Design, trade-offs and integration

François Rigaut,[1]★ Benoit Neichel,[2] Maxime Boccas,[2] Céline d'Orgeville,[1] Fabrice Vidal,[2] Marcos A. van Dam,[2,3] Gustavo Arriagada,[2] Vincent Fesquet,[2] Ramon L. Galvez,[2] Gaston Gausachs,[2] Chad Cavedoni,[2] Angelic W. Ebbers,[2] Stan Karewicz,[2] Eric James,[2] Javier Lührs,[2] Vanessa Montes,[2] Gabriel Perez,[2] William N. Rambold,[2] Roberto Rojas,[2] Shane Walker,[2] Matthieu Bec,[4] Gelys Trancho,[4] Michael Sheehan,[4] Benjamin Irarrazaval,[4] Corinne Boyer,[5] Brent L. Ellerbroek,[5] Ralf Flicker,† Damien Gratadour,[6] Aurea Garcia-Rissmann[7] and Felipe Daruich[8]

[1]*The Australian National University, RSAA, Mount Stromlo Observatory, Cotter Road, Weston Creek, ACT 2611, Australia*
[2]*Gemini Observatory, c/o AURA, Casilla 603, La Serena, Chile*
[3]*Flat Wavefronts, PO BOX 1060, Christchurch 8140, New Zealand*
[4]*Giant Magellan Telescope Organization Corporation, PO box 90933, Pasadena, CA 91109, USA*
[5]*Thirty Meter Telescope, 1200 E. California Blvd., Pasadena, CA 91125, USA*
[6]*LESIA, Observatoire de Paris-Meudon, Place Jules Janssen, F-92190 Meudon, France*
[7]*European Southern Observatory, Karl-Schwarzschild-Str. 2, D-85748 Garching bei München, Germany*
[8]*ALMA, Alonso de Córdova 3107, Vitacura, Santiago, Chile*

Accepted 2013 October 22. Received 2013 October 21; in original form 2013 September 27

ABSTRACT

The Gemini multiconjugate adaptive optics system (GeMS) at the Gemini South telescope in Cerro Pachón is the first sodium-based multilaser guide star (LGS) adaptive optics system. It uses five LGSs and two deformable mirrors to measure and compensate for atmospheric distortions. The GeMS project started in 1999, and saw first light in 2011. It is now in regular operation, producing images close to the diffraction limit in the near-infrared, with uniform quality over a field of view of two square arcminutes. This paper is the first one in a two-paper review of GeMS. It describes the system, explains why and how it was built, discusses the design choices and trade-offs, and presents the main issues encountered during the course of the project. Finally, we briefly present the results of the system first light.

Key words: instrumentation: adaptive optics – instrumentation: high angular resolution – telescopes.

1 INTRODUCTION

Adaptive Optics (AO) is a technique that aims at compensating quickly varying optical aberrations to restore the angular resolution limit of an optical system. It uses a combination of wavefront sensors (WFSs), to analyse the light wave aberrations, and phase correctors (e.g. deformable mirrors) to compensate them. In the early 1990s, astronomers experimented with the technique with the goal of overcoming the natural 'seeing' frontier - the blurring of images imposed by atmospheric turbulence. See Rousset et al. (1990) for the results of the first astronomical AO system, COME-ON, and Roddier (1999) for a more general description of the first years of astronomical AO. The seeing restricts the angular resolution of ground-based telescopes to that achievable by a 10 to 50 cm telescope (depending on the wavelength of the observation), an order of magnitude below the diffraction limit of 8–10 m class telescopes. Two main limitations have reduced the usefulness of AO and its wide adoption by the astronomical community. First, the need for a bright guide star to measure the wavefront aberrations and second, the small field of view (FoV) compensated around this guide star, typically a few tens of arcseconds. The first limitation was solved by creating artificial guide stars, using lasers tuned at 589 nm, which excite sodium atoms located in the mesosphere around 90 km altitude (Foy & Labeyrie 1985). These Laser Guide Stars (LGSs) could be created at arbitrary locations in the sky, thus solving the problem of scarcity of suitable guide stars. Nowadays, all of the

★ E-mail: francois.rigaut@anu.edu.au
† Deceased

major 8–10 m ground-based telescopes are equipped with such lasers (Wizinowich 2012). The second limitation arises from the fact that the atmospheric turbulence is not concentrated within a single altitude layer but spread in a volume, typically the first 10 km above sea level. Multiconjugate adaptive optics (MCAO) was proposed to solve this problem (Dicke 1975; Beckers 1988; Ellerbroek 1994; Johnston & Welsh 1994). Using two or more Deformable Mirrors (DMs) optically conjugated to different altitudes, and several WFSs, combined with tomographic techniques, MCAO provides 10 to 20 times the FoV achievable with classical AO. MCAO as such was first demonstrated by Multi-conjugate Adaptive optics Demonstrator (MAD), a prototype built at the European Southern Observatory (ESO; Marchetti et al. 2008). MAD demonstrated that MCAO worked as expected, but did not employ LGSs and as such could only observe a handful of science targets.

Gemini Multiconjugate adaptive optics System (GeMS) is a MCAO system in use at the Gemini South telescope. It uses five LGSs feeding five 16 × 16 Shack–Hartmann WFSs, and needs three Natural Guide Stars (NGSs) and associated natural guide star wavefront sensors (NGSWFSs) to drive two DMs. It delivers a uniform, close to diffraction-limited near infrared (NIR) image over an extended FoV of 2 square arcmin. GeMS is a facility instrument for the Gemini South (Chile) telescope, and as such is available for use by the extensive Gemini international community. It has been designed to feed two science instruments: Gemini south adaptive optics imager (GSAOI, McGregor et al. 2004), a 4k × 4k NIR imager covering 85 arcsec × 85 arcsec, and Flamingos-2 (Elston et al. 2003), an NIR multi-object spectrograph.

GeMS began its on-sky commissioning in 2011 January and in 2011 December, commissioning culminated in images with a full width at half-maximum (FWHM) of 80±2 mas at 1.65 μm (*H* band) over the entire 85 arcsec GSAOI FoV.

This paper is the first in a two-paper review of GeMS. It makes extensive use of past published material to which the reader is referred.

The plan of this paper follows chronologically the sequence of events in the history of GeMS to date. Section 2 gives a general introduction about the subject of MCAO. Section 3 gives a short overview of how GeMS came to be. Section 4 goes through the design, and discusses the various trade-offs that had to be made, due to cost or technological reasons. The next step after design and construction is the assembly, integration and tests (AITs); these are described in Section 5 which also addresses in some detail the major issues that were encountered during the AITs. Finally, we present and discuss the results of the system first light. This paper is followed by Paper II, which reports on GeMS commissioning, performance, operation on sky and upgrade plans.

2 WHY MCAO?

In the late 1990s, LGS AO systems were emerging but still in their infancy. LGS AO held the promise of boosting the sky coverage accessible for AO compensation to very useful values (typically 30 per cent over the whole sky), but still suffered from two main limitations: anisoplanatism and focal anisoplanatism – aka the cone effect. The cone effect (Tallon & Foy 1990) is a consequence of the finite distance to the LGS (≈90 km above sea level). The effect of focal anisoplanatism on image quality depends on the turbulence Cn^2 profile and the diameter of the telescope. Under typical conditions on an 8 m telescope, the Strehl ratio at 1.2 μm is halved (Fried & Belsher 1994). In addition to the cone effect, angular anisoplanatism degrades the compensation quality when going off-axis from the LGS.

MCAO uses several WFSs and DMs and tomographic-like wavefront reconstruction techniques to extend the correction off-axis, that is, obtaining AO compensation not in a single direction, but over a FoV several times larger than the isoplanatic patch.[1] Thanks to the volumetric probing of the atmospheric turbulence and the tomographic processing, and compared to classical LGS AO, MCAO also virtually eliminates the cone effect (Rigaut, Ellerbroek & Flicker 2000), increases the sky coverage and, by providing a significantly more uniform point spread function (PSF), eases the astronomical data reduction process as well as improves the photometric and astrometric accuracy. MCAO was initially proposed by Dicke (1975) and then by Beckers (1988), and the theory was developed by Ellerbroek (1994). The promises of MCAO attracted the interest of the science community (Ellerbroek & Rigaut 2000; Ragazzoni, Marchetti & Valente 2000), and around the year 2000, two projects started: GeMS (Gemini MCAO System) at the Gemini Observatory and MAD at ESO (Marchetti et al. 2003, 2008).

3 HISTORY OF GEMS

Under the leadership of Ellerbroek (project manager) and Rigaut (project scientist), and once the kick-off effort had been approved by Matt Mountain (Gemini observatory director) and Fred Gillett (Gemini project scientist), GeMS passed a conceptual design review (CoDR) in 2000 May. GeMS was to use three DMs, five LGSs and associated laser guide star wavefront sensors (LGSWFSs), and three NGSWFSs (more details in Section 4.4). It would consist of many subsystems (see Section 4.2); the main optical bench was to be attached to the telescope Instrument Support Structure (ISS), process the beam from the telescope and feed it back to the science instruments. From the beginning, a dedicated large NIR imager (that would become GSAOI) and a NIR multi-object spectrograph (Flamingos-2) were considered. A multi-integral field spectrograph was initially considered but rejected on the basis of cost and object density, which was too low for the Gemini 8 m aperture over a 2 arcmin FoV.

Following the CoDR, the Gemini science community was engaged during a three-day science case workshop in 2000 October at the Center for Adaptive Optics headquarters in Santa Cruz. The workshop gathered 50 participants from the Gemini international astronomy community. Discussions focused on three main science themes: *'Star formation and evolution in the Milky Way'*, *'Nearby galaxies'* and *'Distant galaxies'*, and eventually resulted in a document which once more emphasized the large gains GeMS would bring to existing programmes and the new science it would enable (Rigaut & Roy 2001).

The team at Gemini also worked to advance theoretical knowledge specific to MCAO (Flicker, Rigaut & Ellerbroek 2000; Flicker 2001; Flicker & Rigaut 2002; Flicker 2003).

As early as the CoDR, MCAO was recognized as the most challenging AO instrument ever built. It was relying on technology that was just starting to appear, and was pushing the limits on many fronts. One of the most challenging of these was the sodium laser. GeMS needed five LGSs. Gemini put together a comprehensive strategy to minimize the risks and cost of procuring the 50 W guide

[1] The angle over which the error is lower than $1 rd^2$ is called the isoplanatic angle (or patch if one refers to the area). It varies from site to site and is wavelength dependent. At Gemini South Cerro Pachón it is about 20 arcsec at 1.6 μm.

star laser for GeMS (d'Orgeville, Rigaut & Ellerbroek 2000), including sodium layer monitoring campaigns that were needed to develop more informed requirements for the lasers (d'Orgeville et al. 2002).

After the CoDR, the project proceeded rapidly to Preliminary Design Review (PDR) level, and a successful PDR took place in the Gemini North headquarters in 2001 May (Gemini 2001). The state of the project after the PDR is summarized in Ellerbroek et al. (2003). Sometime after the PDR, it was decided within Gemini to split up GeMS into subsystems, so as to get more tractable subcontracts. The prime motivation was to retain the AIT phase in-house – an important step when considering the complexity of the system and the need for long-term maintainability and upgrades. A number of subsystems were identified, that are listed below in Section 4.2. Consequently, there was no overall system Critical Design Review (CDR), but instead a whole new cycle of PDR/CDR by subsystem, held by the various vendors.

4 DESIGN AND TRADE-OFFS

4.1 Simulations

Initial simulations were carried out by two independent but similar software packages. LAOS, written by Ellerbroek (Ellerbroek & Cochran 2002; Ellerbroek 2002) and AOSIMUL, the precursor of YAO, written by Rigaut (Rigaut & van Dam 2013) are both Monte Carlo physical image formation codes that simulate atmospheric turbulence and AO systems, including WFS, DM, control laws, etc. Broadly speaking, these packages have similar functionalities. Results were cross-checked between the two packages and bugs in the simulation codes were fixed. These simulations were extensively used as input for most of the design choices, such as the order of AO correction, the number and conjugate range of the DMs and so on.

4.2 Subsystems

Post-PDR, a number of subsystems were identified as given below.

(i) The optical bench (Canopus) including all optomechanics and the NGSWFS were built by Electro Optics System Technologies (EOST; James et al. 2003).

(ii) The off-axis parabolas (two F/16 and one F/33) were polished by the Optical Science Center at University of Arizona.

(iii) The LGSWFS assembly was made by the Optical Science Company (tOSC). It has five arms. As in any Shack–Hartmann WFS, there were stringent requirements in pupil distortion and wavefront quality. The particular challenge was to keep distortions and aberrations low for *off-axis* LGS over a wide LGS range (80 to 200 km). Rob Dueck at tOSC went through seven iterations for the optical design, to end up with a solution with eight optics per LGS channel (four are common to the five paths and four are independent per path) and eight actuated stages for the whole assembly.

(iv) The Real-Time Computer (RTC) was also built by tOSC. It uses a dedicated, Operating System-less TigerShark Digital Signal Processor platform (2 × 6 DSPs), with a windows host computer (communications, Graphical User Interface and interfacing with the DSP dedicated PCI bus).

(v) The 3 DMs, DM0, DM4.5 and DM9 (the number refers to their conjugation altitude) were built by CILAS. An important note on the number of DMs: GeMS was designed and integrated with 3 DMs. However, following issues with one of them (see Section 5.3.3), the system has been working with only 2 DMs – the ground and the 9 km DMs – for most of the commissioning. The intermediate DM will eventually find its way back into Canopus. This is why the reader will find throughout this paper sometimes confusing references to the system in both its 2 and 3 DM configurations.

(vi) The DM electronics were built by Cambridge Innovations. CILAS DMs take ±400 V and the phase delay induced by the electronics had to be small at the loop maximum rate of 800 Hz.

(vii) The Beam Transfer Optics (BTO), because of their very tight integration with the telescope and observatory operations were designed and built in-house at Gemini.

(viii) The Laser Launch Telescope (LLT) was built by EOST. LLT is generally considered non-challenging subsystems and too often is not given enough attention. As a result, it often fails, or fall short of the original specifications. Challenges of this subsystem are optical quality, flexure and, more importantly, athermalization to avoid focus drifts in the course of an observing night. Focus drift would result in LGS spots FWHM degradation, which is difficult to measure as they have the same signature than, say, seeing or laser beam size degradation.

(ix) The laser was built by what was initially Coherent Technologies Inc., which turned into Lockheed Martin Coherent Technologies shortly after the contract was signed. Although there were some discussions initially whether it was better to go for five 10 W lasers or one 50 W laser, it soon appeared that even if developments were more challenging, the latter solution was preferable for cost, space and maintenance reasons. Many more details can be found in d'Orgeville et al. (2002), Hankla et al. (2006) and d'Orgeville & McKinnie (2003).

Of paramount importance were the software, the safety systems and the management. The software represented a very significant effort. Functionalities to be provided went from low-level control of hardware (e.g. BTO motors) to adapting the Gemini observation preparation tool for use with GeMS, through the real-time code, the AO simulation, the AO real-time display and diagnostic (RTDD) tool, airplane detection code, satellite avoidance, laser traffic control, etc. Some elements can be found in Boyer et al. (2002), Bec et al. (2008b), d'Orgeville et al. (2012) and Trancho et al. (2008).

The management and systems engineering were done in-house. GeMS has had four project managers in the 13 years span of the project to date; Brent Ellerbroek, Mike Sheehan, Maxime Boccas and Gustavo Arriagada. Boccas et al. (2008) exposes in some details management issues, schedule and resources.

4.3 Sodium monitoring campaigns

To be able to make an informed decision about the laser power requirements, the design team realized early that there was a need for sodium layer characterization at or close to Cerro Pachón. A site monitoring campaign was set up at the Cerro-Tololo Interamerican Observatory (CTIO, operated by the Association of Universities for Research in Astronomy) in Chile in 2001 and 2002. It comprised five observation runs of typically 10 nights each, strategically scheduled every 3 months to get a proper seasonal coverage. Both the CTIO 1.5 m and Schmidt telescopes were used. The goal was to measure sodium layer profile, and derive sodium density, layer altitude and structure on a minute time-scale. The set-up and results are described in d'Orgeville et al. (2003) and Neichel et al. (2013). The laser was a dye laser on loan from Chris Dainty's group at the Blackett Laboratory, Imperial College, London. The power propagated on sky was in the 100–200 mW

Table 1. GeMS in numbers. For acronyms see Section 4.4.3.

DM conjugate range	0, 4.5 and 9 km
DM order	16, 16 and 8 across the 8 m beam
Active actuators	240, 324, 120 (total 684)
Slaved actuators	53, 92, 88 (total 233)
5 LGSWFS	SHWFS, 16 × 16 (204 subap) 2 × 2 pix/subap., 1.38 arcsec/pixel
3 NGS TT WFS	APD-based quad cells, 1.4 arcsec FoV
1 NGS Focus WFS	SHWFS, 2 × 2 Light split with TT WFS #3
WFS sampling rate	Up to 800 Hz
TT WFS magnitudes	3 × R=16 (actual, spec was 18) for 50 per cent Strehl loss in H
LGS const. geometry	(0,0) and (±30,±30) arcsec
Launch telescope	Behind telescope M2, 45 cm ⊘
Wavefront control	Minimum variance reconstructor decoupled LGS/NGS control

range. Results confirmed seasonal variations, with a sodium column density minimum around 2×10^9 atoms cm^{-2} occurring in the Southern hemisphere summer. The GeMS instrument design and the laser requirements were based on this rather conservative value, as summer is the best season to observe, given that statistically speaking it offers better seeing and clearer weather conditions. These data also provided useful information on the sodium layer altitude variations; an important quantity when considering how often the focus information should be updated on an LGS system, using a reference NGS – typically, but not necessarily, the same NGS as for tip-tilt (TT). It was found by d'Orgeville et al. (2003) that the rms variation of the sodium layer mean altitude is of the order of 15 nm over 30 s, thus an integration time of 10 s on the NGS focus WFS would be adequate.

4.4 System description

Table 1 presents a top-level description of the main system components. Fig. 2 shows a diagram of the major subsystems and their interconnections, including the many loops and offloads. These are discussed in more details below.

4.4.1 Laser and laser guide star control

GeMS works with an LGS constellation (see Fig. 1) resembling the five spots on the face of a die: four of the LGS spots are at the corners of a 60 arcsec square, with the fifth positioned in the centre. These LGSs are produced by a 50 W laser split into five distinct 10 W beacons by a series of beam splitters. The on-sky performance of the Laser Guide Star Facility (LGSF) is described in d'Orgeville et al. (2012). The laser bench and its electronics enclosure are housed inside a Laser Service Enclosure, located on an extension of the telescope elevation platform (a Nasmyth focus for other telescopes). The BTO, a subsystem of the LGSF, relays the laser beam(s) from the output of the Laser system to the input of the LLT located behind the telescope secondary mirror. Besides relaying the laser light from the laser to the LLT, the BTO ensures the slow and fast compensation of telescope flexures and constellation alignment control. Fig. 2 shows a diagram of the main BTO elements and their interactions. Because Gemini South is an Alt-Az telescope and because the LGSs are launched from a small telescope fixed on the back of the secondary mirror, the laser constellation must follow the telescope field rotation and de-rotate to keep the LGS spots

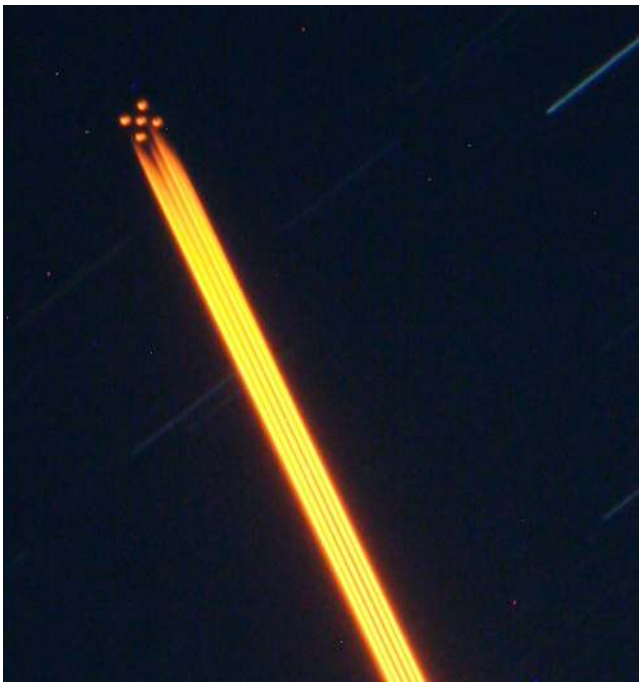

Figure 1. The LGS constellation viewed from the side (about 100 m off-axis) using a 500 mm telephoto lens. The exposure time is 30 s.

fixed with respect to the AO bench. This is achieved by a K-Mirror (KM) located in the BTO. Alignment and control of each LGS in the constellation is provided by five fast TT platforms, called Fast Steering Array (FSA). The FSA platforms offload average TT to a centring and pointing mirror (CM and PM). The averaged rotation accumulated on the FSA platform is also offloaded to the KM.

4.4.2 Laser safety systems

Operating and propagating guide star lasers are delicate. These are Class IV lasers which have very well defined and stringent safety regulations (for good reasons). As far as propagation is concerned, when MCAO operation was first discussed, there was good experience from a few other facilities: namely, the Shane 3 m telescope at Lick Observatory, the Starfire Optical Range in New Mexico and the Keck II telescope on Mauna Kea. On US soil, propagating guide star lasers requires approval from the Federal Aviation Administration (or the local equivalent outside the US), and using a secure and approved system to avoid propagating in the direction of planes; something that was – and still is – performed at Gemini by human spotters. Depending on the local authorities, alternative solutions have been sought, that may involve arranging for a no-fly zone (ideal) or using automated wide field or thermal cameras to detect air planes and automatically stop laser propagation. In the US, it has been historically challenging to obtain authorization from the Federal Aviation Administration (FAA) to replace human spotters by automated systems. However, Gemini gave it a try: hardware was procured, and significant development efforts were dedicated to write plane detection software (Bec et al. 2008b), with good success. Planes were generally detected during test runs, from 10° elevation up (GeMS cannot be used at elevation lower than 40°, so this leaves some margin), with very high probability.[2] This

[2] Note that this is the key word, and 'very high' probability may actually not cut it.

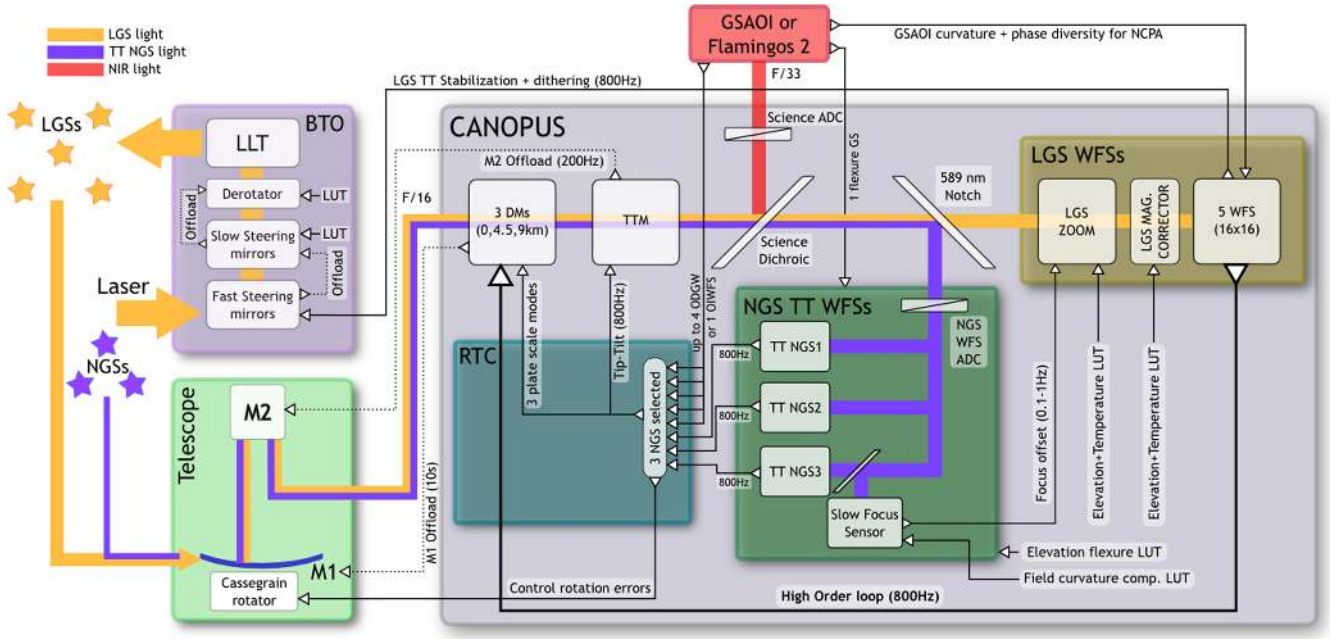

Figure 2. GeMS 'synaptic' diagram, showing major subsystems and their relationship, all loops and offloads.

effort was however cut short before the software was truly a finished product, as it appeared that it would be challenging to obtain approval from the FAA (at Gemini North, or its Chilean equivalent, the Dirección General de Aeronáutica Civil, at Gemini South).

Another agency with which GeMS operations have to coordinate with is the US Laser Clearing House (LCH). This agency coordinates high power laser upward propagation to avoid hitting space assets, e.g. satellite stabilization sensors which could be disturbed or potentially be damaged by the laser light. List of targets have to be sent by the observatory to the LCH, which returns a list of time windows during which propagation is or is not authorized. There are several levels of security (both automated and human) at Gemini during observing to prevent propagating during a LCH no-propagation window. Generally, but not always, the observing plan for the night is put together such as to avoid long no-propagation windows, by the proper selection of targets (no-propagation windows are on a target basis). See d'Orgeville et al. (2008, 2012) and Rigaut & d'Orgeville (2005) for more details on all the laser safety systems.

A third and final concern when propagating lasers is interference with neighbour facilities. Rayleigh scattering of the 589 nm light (or whatever other wavelength in the case of a Rayleigh LGS) can definitely wreak havoc on images or spectra from telescopes situated up to a few kilometres away, so coordination with neighbour facilities – and possibly the establishment of policies – are a must (e.g. should priority be given to the first telescope on a given target or to non-laser telescopes?). The software, initially written by Keck for Laser Traffic Control System at Mauna Kea (LTCS; Summers et al. 2012) was adapted for operation at Gemini South. Currently, the only neighbour telescope is SOAR; studies were done and measurement taken and it was concluded that CTIO (a distance of 10 km as the crow flies) was not affected by Gemini's laser.

4.4.3 Canopus, the optical bench

The optical design was done by Richard Buchroeder (James et al. 2003; Bec et al. 2008a). It is a plane design, intended to simplify

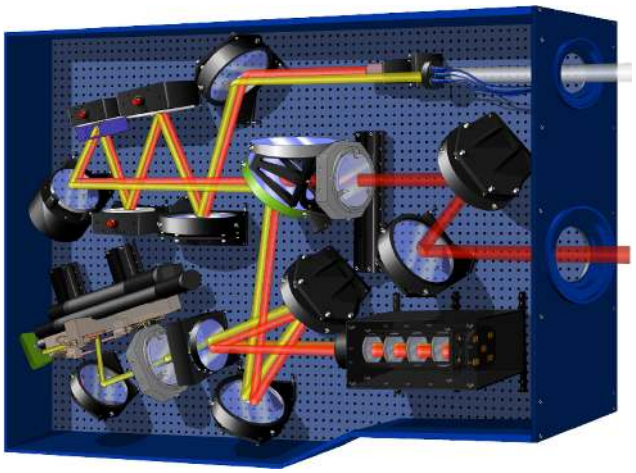

Figure 3. View of the AO optical bench, Canopus.

alignment and maintenance. Fig. 3 shows the (vertical) AO optical bench, Canopus, attached to the Gemini Cassegrain-located ISS. Through the ISS, the Gemini telescope F/16 beam is re-directed to the Canopus bench via the flat AO-fold mirror. The MCAO correction is performed by three DMs conjugated to 0, 4.5 and 9 km (hereafter called DM0, DM4.5 and DM9, respectively) and one tip-tilt mirror (TTM). Following the DMs, a first dichroic beam splitter is responsible for separating visible from NIR light, sending the former to the WFSs, and the latter to the science output with a F/33.2 focal ratio to feed the instruments. The visible light directed towards the WFS is split into a narrow range around 589 nm to illuminate the five LGSWFSs; the remaining visible light goes to the NGSWFS. Fig. 2 provides a complementary, functional view of the entire GeMS system. More details can be found in Bec et al. (2008a).

The whole optical bench is 'sandwiched' on either side by electronic enclosures that house all the control electronics for mechanical stages and calibration sources, as well as the RTC, the DM

high voltage power supplies, the TT mirror control electronics, the Avalanche Photodiodes (APDs) counters and the CCD controllers. The entire instrument weighs approximately 1200 kg and fits in a $2 \times 2 \times 3$ m volume.

4.4.4 LGSWFS and LGS-related loops

The LGSWFS is composed of five 16×16 subaperture Shack–Hartmann. All five LGSWFS are identical, except for their pointing. The LGSWFS pixel size is 1.38 arcsec and each subaperture is sampled by 2×2 pixels (quad cell configuration). The LGSWFS assembly contains eight stepper mechanisms (two zoom lenses and six magnificators) used to accommodate the changes in range of the LGSs (change in telescope elevation or changes in the Na layer altitude), as well as to compensate for flexure and temperature variations present at the ground level. The current range accessible with the LGSWFS is from 87.5 to 140 km, corresponding to an elevation range of 90° to 40°, respectively. The following parameters need to be controlled: (i) the DM0 to each LGSWFS registration, (ii) the WFS magnification and (iii) the focus phase errors. These are controlled using look-up tables (LUT) that depend on elevation, Cassegrain rotator position and temperature (Neichel et al. 2012a).

The LGSWFS provides a total of 2040 slope measurements from 204 valid subapertures per WFS. The use of quad cells require the knowledge of a calibration factor, the centroid gain, to transform the quad cell signal (unitless) into a meaningful quantity, e.g. the spot displacement in arcsec. This centroid gain is proportional to the size and shape of the LGSWFS spot, which changes with laser beam quality, seeing and optical distortions. The calibration of the LGSWFS centroid gains is thus done in soft real time, by a procedure described in Rigaut et al. (2012).

The TT signal from each of the LGSWFS is averaged and sent to the BTO-FSA to compensate for the uplink laser jitter, and it keeps the laser spots centred at a rate of up to 800 Hz. The remaining modes are used to compute the MCAO high-order correction applied at a rate of up to 800 Hz by the three DMs. The total number of actuators is 917 including 684 valid (seen by the WFSs) and 233 extrapolated (Neichel et al. 2010). Unsensed actuators are very important for AO systems with a DM conjugate to an altitude higher than the ground since they affect science targets located in the outskirts of the FoV. The phase reconstruction and DM voltage control is done by a RTC. The reconstruction algorithm is described in Neichel et al. (2010). The RTC also computes the averaged first 12 Zernike modes on DM0 and offloads them to the primary mirror of the telescope at a lower rate.

4.4.5 NGSWFS and NGS-related loops

The NGSWFS consists of three probes, each containing a reflective pyramid that acts like a quad cell feeding a set of four fibres and corresponding APDs. The three probes can be placed independently within a 2 arcmin acquisition field. Each probe provides a tip and a tilt measurement at a rate of up to 800 Hz (capped by the LGSWFS rate). The weighted averaged signal over the probes gives the overall TT and is used to control the TTM. The weights depend on the noise and location of the WFS.

The TTM offloads its average pointing to the secondary mirror of the telescope at a rate of up to 200 Hz. A rotation mode is estimated from the probe positions, and offloaded to the instrument rotator. Finally, the differential TT errors between the three probes are used to control the plate scale modes (also called Tilt-Anisoplanatic or TA modes Flicker & Rigaut 2002). The plate scale errors are compensated by applying quadratic modes with opposite signs on both DM0 and DM9. The reconstruction algorithm follows the scheme described in Neichel et al. (2010). As there is no offloading possibilities for DM9, the position of the probes in front of their respective guide star must be optimized. This is done during acquisition when the TT errors are averaged over a 10 s period, and each of the NGS guide probes is moved in order to lower this error below a given threshold. After setting-up on an object, the individual probes are locked on a common platform, fixing the relative distance between them. During an observation, only the common platform moves, hence conserving the image plate scale and allowing for astrometry measurements.

One of the probes contains a small beam splitter that sends 30 per cent of the light to a slow focus sensor (SFS). As the LGSs are used to compensate for atmospheric focus, any changes in the sodium layer altitude cannot be disentangled from atmospheric focus changes. To cope with this effect, the focus on an NGS is monitored by the SFS. The SFS is a 2×2 Shack–Hartmann and the focus error it measures is sent to the LGSWFS zoom to track the best focus position as seen by the science path. The SFS control strategy is described in Neichel et al. (2012b).

To compensate for potential differential flexures between the AO bench and the instrument, a flexure loop uses the signal coming from an on-instrument WFS on the science instrument. The flexure signal is used to drive the position of the NGSWFSs with an update rate between 1 and 30 s.

4.4.6 Control

The RTC is responsible for measuring and correcting wavefront errors. It was built by Stephen Brown at tOSC and is described in Bec et al. (2008a). The signal from the five LGSWFSs and three NGSWFSs is collected and analysed to control the three DMs and the TTM.

The RTC was built using off the shelf components. A Pentium CPU hosts the graphical user interface and runs miscellaneous background tasks. The host implements the TCP/IP layer to the observatory command and status interface. Hard real-time computations and control of the hardware (5 LGSWFS, 3 DMs, 3 NGS TT WFS and the TTM) are handled by an array of 12 TigerSHARCs DSPs (two TS201S cards hosting six 550MHz DSPs each) mounted on a PCI extension chassis. Distribution of tasks on different DSPs allows a high degree of parallelism. Communication between the different processes in the RTC is accomplished using shared memory. Different ring buffers store real-time information, which can be saved on disk to be accessible to background optimization processes and diagnostic utilities. Stringent operations were implemented in assembly code to meet the high throughput and low latency requirements of GeMS. The overall latency (last received pixel to last command sent to the DM power supply) was measured at approximately 50 μs (see Section 5.2.5).

The LGS control law implements a leaky integrator of the form

$$y[n] = (1 - l)\, y[n - 1] + g\, e[n], \tag{1}$$

where $y[n]$ is the command at time n and $e[n]$ is the wavefront error computed from the WFS slopes. The integrator loop gain is g and l is a leak term required to reduce the effect of poorly sensed modes. The leak turned out to be of utmost importance during the integration and test phase, to be able to work in closed loop even when the system was not perfectly aligned.

The TT control law is given by

$$y[n] = b_1\ y[n-1] + b_2\ y[n-2] + a_1\ e[n] + a_2\ e[n-1], \qquad (2)$$

where a_1, a_2, b_1 and b_2 are coefficients that can be set to reduce the TT error. Some more complex control laws (Kalman, H_2, H_∞) have also been tested for vibration suppression (Guesalaga et al. 2012, 2013), and may be implemented for operation in the future (see Paper II for more details).

GeMS reconstructors were originally generated based on synthetic interaction matrices. Rigaut et al. (2010b) list advantages and drawbacks of this choice. The current scheme is now based on measured experimental interaction matrices. Note that the interaction matrix depends on the zenith angle due to the changing range to the LGSs. A regularized inverse of the interaction matrix is used to reconstruct the wavefront.

Since the RTC hardware was not specified to perform two matrix multiplies, pseudo-open-loop control is not possible. Therefore, true minimum-variance reconstructors cannot be implemented.

4.5 Software

This section focuses on the high-level software associated with Canopus operation. For information concerning the BTO, laser and laser safety systems software, the reader is referred to d'Orgeville et al. (2012, 2008).

4.5.1 High-level control and display

MYST is the top-level engineering graphical user interface for the operation of Canopus. It has been described extensively by Rigaut et al. (2010a). As a GUI, MYST essentially fulfils two functions: it provides convenient control of the Canopus functionalities (loop control, mechanism control, control matrix creation, etc.) and an RTDD tool. The RTDD can display raw (WFS slopes, DM actuators, etc.) and processed (e.g. DM projection on Zernike modes, r_0 estimation by fitting of Zernike mode variance) information at 10–20 Hz. Fig. 4 gives an example of what the RTDD looks like (pull down menus allow independent configuration of each graphical pane).

4.5.2 Offline packages: data reduction and calibrations

In addition to MYST, a number of high-level software packages were developed for offline data analysis or calibration.

(i) WAY is a generic wavefront reconstruction and display tool and was used with the 24x24 diagnostics Shack–Hartmann WFS used during the AIT (Garcia-Rissmann et al. 2010).

(ii) OPRA (Gratadour & Rigaut 2011; Rigaut et al. 2011) is a phase diversity package that uses the new tomographic method described in Section 5.2.2. It is used regularly since the beginning of the commissioning (needs both Canopus and GSAOI) to null non-common path aberrations.

(iii) YAO (Rigaut 2002; Rigaut & van Dam 2013) is a software package and library to simulate AO systems. It is derived and expanded from AOSIMUL (See Section 4.1). It was used extensively, as the library that power other tools (MYST, WAY), as a simulator to interface with the other software tools for testing, and finally and most importantly, to generate synthetic control matrices for the system when this method was in use.

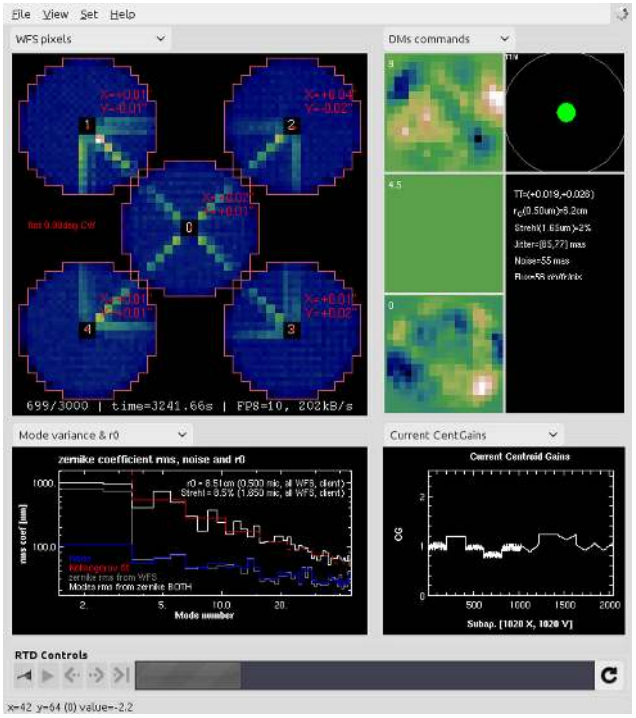

Figure 4. Snapshot of the real-time display and diagnostics in action.

(iv) ASCAM (Bec et al. 2008b) is the software package developed and tested at Gemini for the detection of moving objects (also works for UFOs), as referred to in Section 4.4.2.

All of these packages make use of either PYTHON, C/C++, YORICK or a combination of these.

4.5.3 Low-level software

Low-level software include the RTC code (Bec et al. 2008a), the Canopus mechanisms control code, the BTO code and the laser safety code (d'Orgeville et al. 2012). The RTC has been described in Section 4.4.6. Control of essentially all the motorized stages and status information from a variety of sensors mounted on Canopus and the BTO is implemented using the Experimental Physics and Industrial Control System (EPICS; Dalieso et al. 1994). EPICS is a standard framework adopted at Gemini. It provides low-level drivers to control hardware (motor controllers, digital and analog input/output etc.), a network transparent layer (Channel Access) to distribute command and status information, a variety of graphical user interfaces builder to generate high-level applications. Approximately half of this software was done in-house. The other half was contracted out to the UK-based company Observatory Science Limited.

4.6 Design choices and trade-offs

During the design phase, a number of choices and trade-offs had to be made; either specific to AO, LGSs, or the multi-LGS, multiconjugate aspect. Because GeMS is still to date the only LGS MCAO system ever built, it is interesting to comment further on these trade-offs.

(i) *Reflective design*. This one is easy enough. As for many AO systems, because of the wide wavelength range (from 450 nm to

2.5 μm), a refractive design for the common path optics would have been very challenging, especially in terms of optical throughput (chromatism correction and coatings).

(ii) *Two output F-ratios*. There was an intense debate about the choice of F/33 for the science output. This was going against the philosophy of Gemini in which the AO was just an adapter and should deliver the exact same F/16 beam as the telescope to the science instruments (as Altair was for instance doing at Gemini North). Eventually, it was recognized that going for F/33 would lower the risk of non-common path aberrations (smaller optics) and actually fit better existing instruments (provide twice the plate scale) and would make the design of AO-dedicated instruments like GSAOI simpler.

(iii) *Lower actuator density on DM9*. In MCAO, because of the FoV, the area to be controlled is larger on high-altitude DMs/optics than in the pupil. For instance, DM0, conjugated to the telescope pupil, has to 'control' an equivalent area of 8 m in diameter. Now when getting to 9 km, the equivalent area (for the GeMS field of 2 arcmin) becomes $8 + 2 \times 60 \times 9\,10^3 \times 4.8\,10^{-6} = 13.2$ m in diameter. This means $(13.2/8)^2 = 2.7$ times the area, for a slab of turbulence that contains a much smaller fraction of the turbulence that what is at the pupil/ground. For cost and complexity reasons, it was thus decided to double the actuator pitch on the highest DM. This should still deliver adequate phase variance reduction, provided of course that the outer scale of turbulence in this high-altitude slab was of the same order as it is in the ground layer, something that was unknown at the time (and still is).

(iv) *Field of view*. The MCAO science case clearly showed that the largest possible FoV (>1 arcmin) was of the utmost importance for the majority of the science cases. This pushed towards a large FoV. Factors that limited the design ambitions included (a) the feasibility and cost of the GSAOI detector array (4k × 4k, in a 4 Hawaii-2RG detector package), given the need to approximately sample at J band (≈20 mas pixel^{-1}) and (b) the fact that the ISS, as built, only transferred a 2 arcmin field through the AO port. The latter constraint would have been very difficult and costly to remedy. Finally, the design team adopted a 2 arcmin maximum FoV, with a central 85 × 85 arcsec over which the compensation quality would be maximized.

(v) *TTM not at the pupil plane*. The TTM is conjugated at about 3 km below ground. The conjugated altitude is not by itself a problem (TT will be corrected the same whatever the conjugation altitude is), but the fact that it is located in-between the DMs and the WFS implies that when it tilts, the TTM will move the image of the DM as seen by the Shack–Hartmann WFS, and thus modify the DM-to-lenslet registration. However, the induced misregistration, e.g., DM0 is only 4 per cent of a subaperture per arcsecond of TTM motion, and was deemed acceptable considering the added complexity, cost and loss in throughput of an optical design where the pupil would have been re-imaged on the TTM.

(vi) *Laser launch behind M2*. In GeMS, there is only one LLT to launch the five LGS beams, and it is located behind M2. The drawback is that in this configuration, any WFS sees the Rayleigh scattering from the other LGS beams (see for instance the upper left WFS display in Fig. 4 and its X pattern of Rayleigh illuminated subapertures). The alternative of using side launched lasers was not seriously considered for the following reasons. It was believed that image elongation resulting from a side projection was very bad in terms of signal-to-noise ratio (SNR) (we know differently since then; Thomas et al. 2008; Robert et al. 2010). Also, entirely avoiding Rayleigh backscatter would have meant (a) getting rid of the central LGS, which at the time was deemed to improve significantly the uniformity across the FoV and (b) using four LLTs, which would have meant a large increase in cost and operation reliability. At the time, it was also believed, due to the absence of any measurements, that the fratricide could be subtracted away from the affected subapertures. This is not feasible, in part because of aerosol and fast laser power variability, but primarily because the BTO uplink pointing adjustment mirrors are not in a pupil plane, causing the Rayleigh (near field) to move when the LGS pointing changes (Neichel et al. 2011b). A last factor was a lower sodium coupling coefficient than initially expected (between the laser and sodium atoms), which reduced the ratio between the LGS and the Rayleigh components. Rayleigh backscatter disables about 20 per cent of the subapertures, but the impact on performance has not been well studied.

(vii) *Number of LGS*. This was based on an exhaustive study using both Ellerbroek (Ellerbroek & Cochran 2002; Ellerbroek 2002) and Rigaut (Rigaut 2002) simulation codes, and driven by both Strehl and Strehl uniformity requirements. In retrospect, it may have been preferable to break the redundancy in the constellation geometry, to avoid or reduce the appearance of invisible modes. Although these do not appear to be much of a problem in the current two DM configurations (see Section 5.3), it could become so when DM4.5 makes its way back into Canopus.

(viii) *Number of NGS*. Alternative schemes to compensate for anisoplanatism TT modes (TT but also plate scale) were looked into (Ellerbroek & Rigaut 2001), for instance using a combination of sodium and Rayleigh laser beacons. Eventually, the simplest method of using three NGS was retained. Detailed sky coverage evaluation showed that the need for three NGS – compared to one for LGS AO – is not detrimental, as the three TT NGS can be located much further away (up to 60 arcsec) than the single TT NGS in LGS AO (up to 30 arcsec typically) for comparable performance (e.g. Fusco et al. 2006).

(ix) *Quad cells*. At the time GeMS was designed, the detector market looked a lot different than it does right now. To fit 16 × 16 Shack–Hartmann spots, the best available low noise detectors were the EEV CCD39, with 3.5 electrons read noise. These CCDs have 80 × 80 pixels, so could only fit 4 × 4 pixels per subapertures. It was thus decided to go for quad cells (2 × 2 pixels) in each subaperture, and keep one guard pixel on each side to avoid cross-illumination between subapertures (combined with a field stop). Quad cells come with a lot of issues though: pixel edge diffusion degrades the FWHM and thus the SNR (Section 5.3.1); but the main issue is centroid gain calibrations. The centroid gain is the constant of proportionality between the quad cell measurement and the physical spot displacement. It is also a function of the spot size and shape. During operation, because of changes in seeing, in laser beam quality, and in the sodium layer thickness/profile, the spot size and thus the centroid gain will change. An inordinate amount of effort was devoted to centroid gain calibration and/or issues related to centroid gains. If there is one lesson learned from GeMS, it is this one: do not use quad cells in a Shack-Hartmann WFS if you can avoid it.

(x) *DM altitude conjugation*. The DM altitude conjugation choice was made based on initial numerical simulations. In particular, there was some debate regarding the number of DMs (two versus three). For the given FoV and targeted wavelengths, the 3 DM configuration was found to be significantly more robust to changes in the Cn2 profile and was finally adopted. Based on more recent measurements derived from GeMS itself, (Cortés et al. 2013) it appears that 9 km is too low to compensate for the turbulence induced by the jet stream, usually located between 11 and 12 km. This is

particularly impacting performance when the telescope is pointing at low elevation and the apparent distance to the jet stream is larger.

5 ASSEMBLY, INTEGRATION AND TESTS

AITs of Canopus took place at the Gemini South based facility, in La Serena, Chile. The first elements were received in 2007, and integration was completed by the end of 2010, when Canopus was sent to the telescope. All the subsystems were assembled and tested in the lab during that period. No formal and overall acceptance test was performed before sending the instrument to the telescope. A good overview of the activities and performance of the system can be found in Boccas et al. (2008), Neichel et al. (2010) and Garcia-Rissmann et al. (2010). Below we summarize the main results obtained during this Canopus AIT period.

5.1 Beam transfer optics

5.1.1 Optics

Construction and integration of the BTO started in 2007, and finished in summer 2010. Integration of the BTO optomechanics on the telescope, with its 32 optics and 26 motors, took a very significant amount of resources. Given its tight integration with the telescope, telescope access time also turned out to be an issue, as it was competing with maintenance, day time instrument calibrations, etc.

The LLT was installed on the telescope in late 2007 (d'Orgeville et al. 2008), and first optical quality measurement was done on-sky soon after. The Gemini South BTO throughput was measured to be of the order of 60 per cent. This is under the original specification of 75 per cent, and was attributed in large part to suboptimal BTO coating specifications that failed to take into account proper polarization control considerations.

5.1.2 Mechanics

Inelastic flexures, probably due to the long length of the BTO, are preventing the use of only LUT to keep the alignment. Active control based on an optical feedback from pre-alignment cameras and the laser pointing on the sky (see Sect. 4.4.1) is mandatory to keep the beams perfectly aligned all along the long BTO optical path. The original BTO design also included a fast Laser Beam Stabilization system that would compensate for vibrations and fast laser beam drifts in the BTO while propagating at full power. It appeared that this real-time stabilization was not required and that only the remote re-alignment mentioned above was enough to keep the alignment on the BTO. Finally, the main issue with the mechanical performance of the BTO was related to the mount of the FSA mirrors. The original mechanical design included a clamping of the piezo body of these TT platforms, causing an accelerated failure rate. This assembly had to be completely rebuilt in 2011, and no failure occurred since the new design has been implemented.

5.2 Canopus

5.2.1 Optics

One of the major difficulties in the original optical alignment of Canopus was to adjust the focus of each optical path (LGS, NGS and science). The constraints are: (a) the LGSWFS zoom should be able to span a range from approximately 87 to 140 km (that is, covering all possible range to the sodium layer from zenith to an elevation of 40°); (b) the science focus is fixed by the GSAOI detector, which is not adjustable in focus; (c) the NGSWFS focus is fixed by the position of the mechanical assembly, which can be manually adjusted by few millimetres (see Fig. 3). Fine adjustments of the Off-Axis Parabola (OAP) position were also necessary to adjust the three focuses simultaneously, while keeping the 2 arcmin field clear of any vignetting and the non-common path aberrations within the required level.

The LGS path throughput (from the entrance shutter of Canopus to the LGSWFS CCD, not including the quantum efficiency of 0.8) was measured in the lab to be 35 per cent at 589 nm. The split is about 65 per cent for the LGSWFS itself (20 optical surfaces at 98 per cent each) and 55 per cent for Canopus common path + WFS path. Admittedly, this is on the low side and could be improved in the future. The optical quality, including elements from the input focal plane calibration sources to the LGSWFS lenslets, is of the order of 250 nm of astigmatism (averaged over the five LGS paths). Differential focus and astigmatism between the five paths were an important issue during the AIT and later on during commissioning. Differential focus was compensated by adjusting the individual collimators in the LGSWFS in 2012. Differential astigmatism cannot be corrected, and should be included in the non-common path aberration (NCPA) compensation procedure.

The optical quality in the NGSWFS was also estimated: NGS spot sizes of about 0.3–0.4 arcsec in all three probes, which were measured when using diffraction-limited calibration sources. NGS spots are slightly elongated, most probably due to residual astigmatism of the order of 150 nm rms, combined with defocus. However, there is no optical element in the NGSWFS path which can be used to compensate for residual aberrations. Due to design errors and alignment issues, the NGSWFS suffers from more than two magnitudes of sensitivity loss. Most of the light loss is happening at the injection of the light into the fibre, and the coupling between the fibre and the APDs. New APD modules were purchased and installed in 2011, providing a better fibre/APD coupling which resulted in a gain of about 1.5 times in flux. A new fibre injection module has also been designed and implemented for one of the probes (C1) but failed to bring the expected improvement and was subsequently removed.

Finally, the image quality in the science path was measured with a high-order WFS in the lab, and then directly on the science camera when at the telescope (see Section 5.2.2). A fine adjustment of the output OAP was performed in order to reduce astigmatism in the science path. Without any NCPA compensation, the raw optical quality of the science path gives *H* band Strehl ratios of the order of 15 to 30 per cent over the 2 arcmin field. With the NCPA, this number goes up to about 90 per cent, as will be seen in Paper II.

The system end-to-end throughput (from outside the atmosphere to the GSAOI detector included) was measured to be 36 per cent in *H* (more details in Carrasco et al. 2012), 21 per cent in *J* and 31 per cent in *K*, better than the initial design value of 23 per cent for all wavelengths.

5.2.2 Non-common path aberration compensation

Of the multitude of calibrations that have to be done with an AO system (and even more so with an MCAO system), the calibration and compensation of static non-common path aberrations (NCPA) is one of the most important. As the name says, those aberrations arise in the paths that are non-common, i.e. generally speaking after the light split between science and WFS paths. Science path aberrations

are not seen by the AO WFS and thus not compensated; the WFS path aberrations are seen of course, therefore compensated, while they should not be as they do not affect the science image directly. These aberrations are compensated by using WFS slope offsets. The difficulty consists in calibrating these aberrations: a wavefront sensing device in the science path is needed. The aberrations measured in the science path are compensated by adding – in software, e.g. using slope offsets – the inverse aberrations to the AO WFS.

In GeMS, the problem is more complex; the goal is to compensate for NCPA over the entire FoV *simultaneously*. Because in the general case aberrations are not constant over the FoV, they also have to be calibrated and compensated depending on the position in the FoV. Several different methods were tried to perform this task; eventually, we settled on an improved version of the method proposed by Kolb (2006). This novel approach (Gratadour & Rigaut 2011), called Tomographic Phase Diversity, is similar to the Phase Diversity + Tomography proposed by Kolb, except that instead of solving for the phase in each individual direction and then solving the tomography with the individual direction phases (to find the tomographic phase correction to apply to individual DMs), one solves directly in the volumetric phase space, using the many individual PSFs as input to the phase diversity process. This method provides better stability and has improved SNR properties compared to the original method proposed by Kolb. Results are given in Paper II.

5.2.3 *Cooling*

A major engineering effort was required to re-design the thermal enclosures of the Canopus electronics, particularly to manage the heat load of the Deformable Mirror Electronics (DME), 2900 W accounting for about 70 per cent of the total 4100 W heat waste to be extracted from the instrument. Because the DME components are particularly sensitive to over temperatures this called for a complete and thorough redesign using new heat exchangers, high performance DC fans, compressed dry air, active valves and new telemetry to monitor the enclosure environment, electronics temperatures and any risk of condensation. The local turbulence in the bench is of the order of $r_0(500\,\mathrm{nm}) = 4\,\mathrm{m}$, which proves that the thermal insulation is effective.

5.2.4 *Mechanics*

Overall, the mechanisms and motors in the AO bench are performing well. The positioning reliability of the LGSWFS stepper motors was checked by taking measurements of DM0 to lenslet pupil registration when moving the bench between 0° and 54° over 50 cycles. The motors performed reliably and under specification in those tests, keeping the average misregistration below 4 per cent (peak to valley) of a subaperture in all beams. Residual flexure is compensated by an LUT. No other flexure – including differential flexures between the different paths – was detected. Drift is mainly caused by temperature: the LGSWFS optical axis moves by approximately 200 mas per 1°C of temperature change. When working with the bench calibration sources, this precluded the utilization of the TTM for centring the LGSWFS when operating with above a certain range of temperatures ($\Delta T \simeq 5^\circ$ C), given that the TTM full range is only 2.8 arcsec. A mechanical stage to adjust the position of the calibration sources along the drifting axis was added in order to compensate this issue.

During the design phase, special care was taken to reduce the impact of vibrations, using rigid, fixed optical mounts, for instance. The level of vibrations measured in the lab, and when the final cooling solution was operational (see Section 5.2.3), was fully acceptable, at the level of 2 and 5 mas rms along the two WFS axis. Vibrations measured on the telescope are slightly larger, of the order of 2 and 7 mas rms, with some clearly identified peaks at 12 and 55 Hz (Neichel et al. 2011a). Occasionally, this goes up to 10 mas rms, e.g. when the cryocooler are pumping hard to cool down an instrument.

5.2.5 *RTC and loops*

The high-order and TT loop behaviour (latency and bandwidth) were calibrated during the AIT period. Measuring the error transfer function on real signal (e.g. noise) is a very powerful tool to characterize the end-to-end properties of such dynamical systems made of optical, mechanical and electronic components. It allowed us to discover (and subsequently fix) a bug in which TT measurements were buffered and used with a one frame delay. Once this problem was fixed, an excellent agreement was found between model and experimental data.

The high-order loop latency (defined here as the delay between the last pixel received from the LGSWFS CCDs and the last command applied to the DM) was measured to be 50 μs. When adding 1.25 ms of read-out time, this results in a total delay of 1.3 ms. The DM response time was found to be negligible (except for failing actuators, see Section 5.3.3), which is what was expected from the manufacturer data. For the TT loop, the main factor limiting dynamical performance is the TTM mechanical behaviour. From manufacturer data (Physik Instrumente), the TTM has a −3dB point at 300Hz, which is in full agreement with our measurements. Overall, when running with maximum gains, the 0dB bandwidth (0dB point in the error transfer function) was measured to be approximately 53 Hz for the high-order loop and 40 Hz for the TT loop.

5.3 Issues and lessons learned

Not surprisingly, because GeMS was the first instrument of its kind, its development encountered a few issues, discussed below.

5.3.1 *WFS CCD pixel modulation transfer function*

As explained in Section 4.6, there are only 2×2 pixels per LGSWFS subaperture, each 1.38 arcsec in extent. The pixel extent was chosen as a compromise between spot clipping by the subaperture FoV (in case of bad LGS spot quality or bad seeing) and degradation of the spot FWHM (and thus the SNR) due to broadening of the spot by the detector pixel Modulation Transfer Function (MTF). Indeed, CCD pixels do not have abrupt edges. Through a phenomenon called pixel edge diffusion, there is a finite probability that a photon falling within the boundaries of a pixel be detected by a neighbouring pixel instead (see e.g. Widenhorn, Weber-Bargioni & Blouke 2010).

By measuring the subaperture centroid gains (proportional to the FWHM, with a factor of proportionality depending on the assumed spot shape), and knowing the calibration source angular size, one can calculate the difference. Typical centroid gains obtained in the lab are 0.7, translating into equivalent FWHMs of 1.3 arcsec (this is subaperture dependent, but turned out to be relatively uniform). Given that the LGS calibration source size is 0.8 arcsec, the degradation kernel is 1.0 arcsec which, after having eliminated other possible sources (e.g. defocus), we attributed to a MTF degradation by the detector. This value of 1 arcsec for the FWHM equivalent of

the MTF degradation kernel, or about 2/3 of a pixel, is not uncommon and matches values measured in dedicated experiments with similar thinned detectors (van Dam, Le Mignant & Macintosh 2004; Widenhorn et al. 2010). This issue could not be remedied with the current EEV-CCD39. An obvious solution would be to upgrade the detectors to low read-out noise larger arrays, thus smaller pixels to sample properly the LGS spots. Such an upgrade is not considered to date, primarily because there are more serious issues to correct first.

5.3.2 BTO design, LGS spot optical quality and brightness

Although the BTO is made of relatively simple optics such as planar mirrors, lenses, beam splitters, and polarization optics, it has proven to be a fairly complex system to align and optimize. One of the main issue that was encountered with the BTO was the location of the FSA mirrors used to compensate for the fast up-link seeing. In GeMS, these five TT platforms are not located in a pupil plane (the LLT primary mirror), inducing a continuous jitter of the laser beam footprints on the LLT primary mirror. When static alignment of the five beams on the LLT is not perfectly done, i.e. when the five beams are not perfectly superimposed on the LLT, the risk of vignetting one or more of the beams is high. Moreover, some variations of the spot quality between the beams is observed, of the order of 0.1 to 0.2 arcsec. This effect is attributed to LLT pupil aberrations and mainly caused by the LLT OAP mounting issues. Finally, not only will projected laser power and spot size per LGS vary over time, but the Rayleigh beam footprints on each LGSWFS (called fratricide) will also change rapidly, making it impossible to ever subtract the Rayleigh background from the LGSWFS frames as well as creating all sorts of spurious effects for the AO reconstructor.

5.3.3 Failure of actuators on DM0

When DM0 was first installed in Canopus, all its actuators were functional. Over two years of AIT work in the lab (2008/2009), three actuators failed – i.e. either they did not react or reacted very slowly. This failure mode is a feature of the DM itself and not of its power supplies. After moving Canopus to Cerro Pachón, actuators started failing more rapidly: six months later, 16 more actuators were non-functional and an actuator was lost every 10 d in average. Although DM4.5 and DM9 did have some dead actuators, they did not show such an accelerated degradation as DM0. Entering the GeMS shutdown during the winter 2011, it was thus decided to replace DM0 with DM4.5, and to replace DM4.5 with a flat mirror.

This has some side effects; positive ones were that it would make the control easier (two instead of three DMs) and that the static shape of DM4.5 was better than DM0, which showed some cylinder due to ageing. Negative ones were to reduce somewhat the expected system performance, given that the total number of active actuators was reduced from 684 to 360, and that the compensation of altitude layer was now effectively handled solely by DM9, with a rather modest actuator pitch of 1 m.

5.3.4 NGSWFS APDs feed

APD-based TT quad cell WFS are the norm in LGS AO systems. STRAP, an APD-based system developed by ESO (Bonaccini et al. 1998), is in use at the ESO VLTs/VLTI, at the Keck I and II telescopes and at Gemini North amongst others. Because of the need to have three TT WFS with adjustable positions within a 2 arcmin FoV, Strap was not an option for Canopus. A three-probe system was designed by EOST, using focal plane pyramids to dissect the focal plane image, and then direct it to fibre-fed APDs. These systems proved extremely difficult to align: they had to be very compact to fit and avoid collisions in the NGSWFS focal plane, which thus prevented implementing the necessary alignment adjustments. Significant effort has been applied to upgrade these systems, with little success. A total redesign based on a single large focal plane array is being planned (see Paper II), which should allow GeMS to reach an NGS limiting magnitude of $R = 18.5$, as was originally specified.

5.3.5 Differential field distortions science/NGS

Two-off-axis parabola systems are widely used in AO. They provide clean pupil re-imaging, with little pupil distortion. They transport the focal plane with very little aberrations over the generally small AO FoV. However, they introduce a significant amount of distortion in the output focal plane. In the science focal plane, field distortions have minor consequences, since they can be calibrated out. In the TT NGS focal plane, this has serious consequences, the most severe of which is that the star constellation will deform when dithering (dithering is the normal mode of observation in the infrared). The TT WFS had been designed with probes #1 and #2 mounted on top of probe #3. The intent was to be able to dither with a motion of probe #3 only, and thus not deform the constellation, to be able to stack science images without having to correct for plate scale between them. The field distortion prevents that. In fact the distortion is so large that dither of 10 arcsec or so will induce differential motion of the order of 0.1–0.2 arcsec between probes, which makes operation impossible and mandate going through another acquisition to centre the probes on their respective stars.

The proposed redesign of the TT WFS mentioned above (see also Paper II) will solve this problem, as the distortion model can be easily incorporated into the positioning model for each guide star on the focal plane array.

5.3.6 Lessons learned

Based on the experience acquired by the team, this section gives a top level list of lessons learned.

Below are the items that caused the most trouble, either because they are limiting performance and/or because they caused very large overheads during AIT and/or commissioning (note that at the time of the GeMS design there was no alternative for most of these choices). All of these issues have been discussed at length earlier in this paper.

(i) LGSWFS quad cells, for two reasons: pixel MTF (performance degradation) and centroid gains (performance degradation and huge calibration burden). Today's alternative is to use large electron-multiplying charge coupled devices to adequately sample Shack–Hartmann spots.

(ii) NGSWFS probes: beware of fibre feeds, mechanism (re)positionnings and guide star catalogue coordinate errors. Today's alternative is to use detector array(s): no moving parts, less optical elements should result in better performance, much simpler calibrations and a huge simplification of acquisition. If this is done properly, one can probably live with the distortion introduced by the two off-axis parabola relay.

(iii) Laser centre launch, for two reasons: first, the fratricide turned out to be a real problem. In GeMS, but probably more

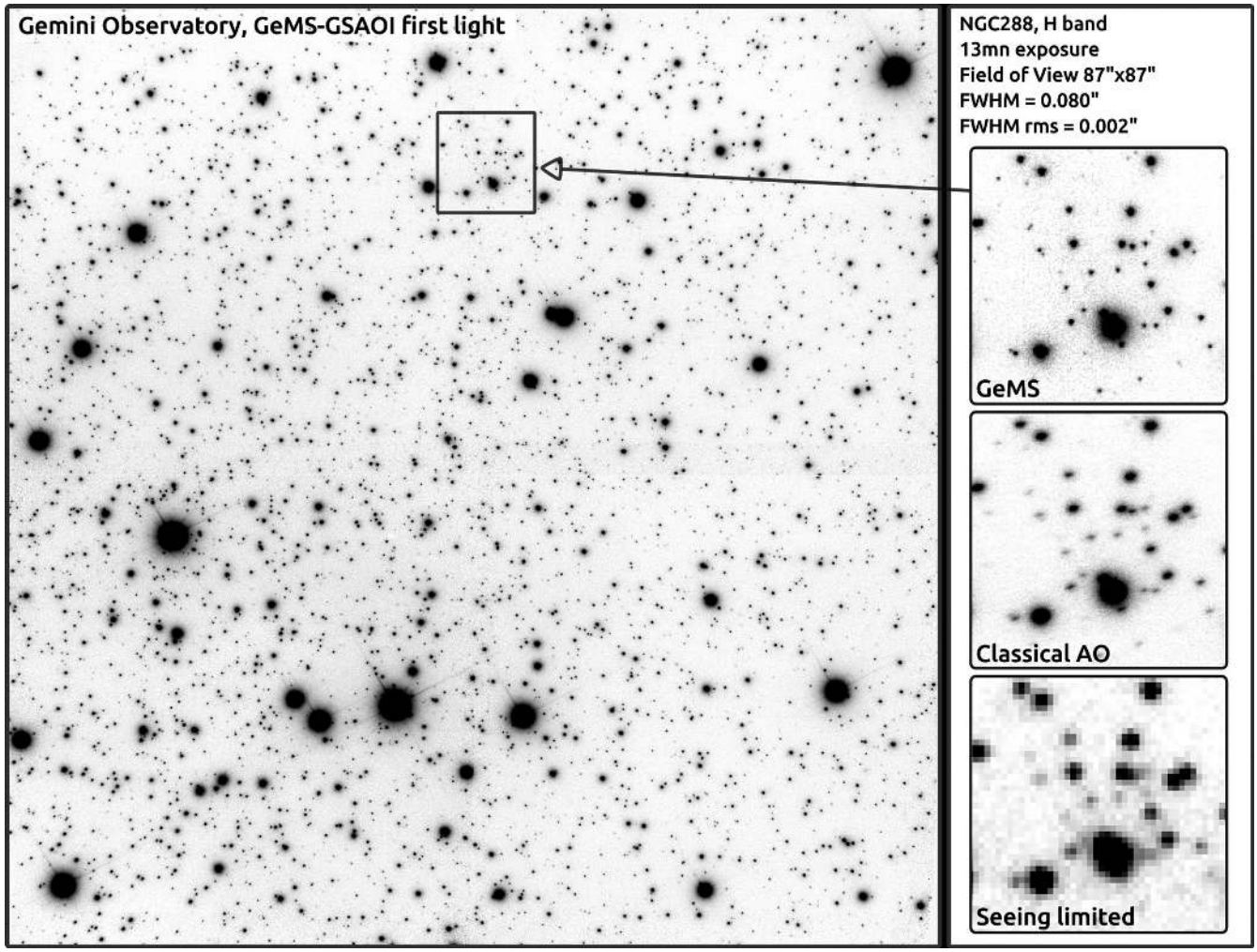

Figure 5. GeMS first light: NGC288 in *H* band.

generally, the Rayleigh scattering cannot be calibrated out. Secondly, because it implies a more complicated BTO relay, with many more optical elements and motors. In fact, the whole BTO, because of its complexity, has implied huge calibration overheads (e.g. constellation alignment). The lesson here is to simplify the BTO design as much as possible. Today's alternative is to use more compact lasers and/or side launch.

(iv) Laser: even though it is a technological feat, GeMS's laser is a very large, costly and complex system. Today's alternative are Raman fibre lasers or Optically Pumped Semiconductor Lasers.

(v) Higher conjugation altitude of high DM.

What worked well, and would be done the same way:

(i) optical design and instrument packaging,
(ii) FoV and constellation geometry,
(iii) reduced actuator density on high-altitude DM,
(iv) AIT in-house and commissioning format (see Paper II),
(v) strong in-house AO team that take control of high-level software and control.

Lessons learned have also been discussed at length in Rigaut et al. (2011, section 3).

6 FIRST LIGHT

Paper II describes in detail the commissioning, operation and performance of GeMS. This section only provides a summary of first light results.

Commissioning took place over the course of 2011 and 2012. The so-called 'first light' image was obtained on 2011 December 16 on the globular cluster NGC 288, and is shown in Fig. 5. The seeing was 0.7 arcsec on this night, close to the median seeing for the site. This image is taken at 1.65μm (*H* band) and has a FoV of 87 arcsec × 87 arcsec. It is a combination of 13 images of 60 s each. The average FWHM is slightly below 80 mas, with a variation of 2 mas across the entire image FoV. Insets on the right show a detail of the image (top), an image of the same region with classical AO (middle; this has been generated from the top MCAO-corrected image and assumes using the star at the upper right corner as the guide star) and seeing-limited observations (bottom). The pixel size in the seeing-limited image was chosen to optimize SNR while not degrading angular resolution.[3] North is up, east is right. Strehl ratios

[3] Keeping the same pixel size as the MCAO image would have resulted in a lot of noise in the seeing limited image, hence to present a fair comparison, we choose to use larger pixels, also more realistic, to generate the seeing limited image.

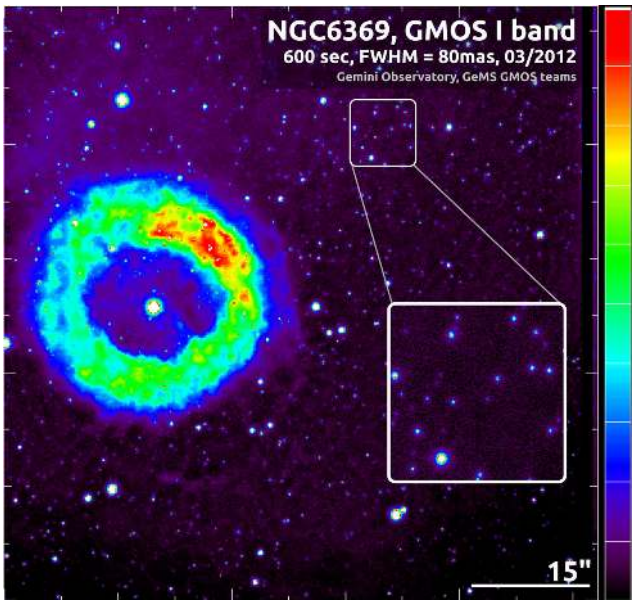

Figure 6. GeMS and GMOS: NGC6369 at *R* band.

across the image are of the order of 15 to 20 per cent. The relatively large FWHM, compared with what has been obtained more recently, can be explained in part because the plate scale and the focus stabilization loops were not closed. Nevertheless, the nicely packed PSF, approximately Lorentzian in shape and without marked halo, is extremely uniform across the 87 arcsec field, demonstrating the very point of MCAO.

Fig. 6 shows a single 600 s exposure of the planetary nebula NGC 6369 acquired with the Gemini Multi-Object Spectrograph (GMOS) in the red, at *I* band (about 830 nm in this case) on 2012 March 14. The FoV is 75 arcsec × 75 arcsec. The natural seeing at the time was between 0.3 and 0.4 arcsec; the FWHM of the corrected image over the displayed field is between 80 and 90 mas. Using GMOS with Canopus has never been very high in the observatory priorities as it was believed that performance was going to be marginal. This image, with about 80 mas FWHM over most of the 2 arcmin FoV unvignetted by Canopus, proves that when the seeing cooperates, GeMS can deliver down the red part of the visible spectrum. This image was the best obtained with GMOS though. Under median seeing conditions, GeMS provided typically a factor of 2 to 2.5 improvement in FWHM, which is roughly what was expected (i.e. slightly better than Ground Layer AO).

Rigaut et al. (2011, 2012) report on additional first light results: FWHM and Strehl ratio uniformity maps and a preliminary error budget; Rigaut et al. (2012) go on with an identification of the factors limiting performance at the time of the first light: photon return (i.e. mostly due to low laser power projected on sky) and generalized fitting (a consequence of the missing DM4.5). Static aberrations were also a problem at the time of first light but has been fixed since then. Finally, the same paper gives a preliminary analysis of the astrometric performance, showing that submilliarcsec accuracy can be readily achieved, and that MCAO is not introducing uncontrolled terms to the astrometric error budget. This was later confirmed by Lu, Neichel & Rigaut (2013), who finds that 0.1–0.2 mas astrometric accuracy can be reached.

Since first light, GeMS has acquired many new stunning images. A collection of legacy images taken on various objects ranging from the Orion nebula to the galaxy cluster Abell 780, through globular and open clusters has recently been published on the Gemini observatory website (http://www.gemini.edu/node/12020). Fig. 7 shows one of these legacy images: the antennas galaxies (NGC4038/39) as seen by the *Hubble Space Telescope* (*HST*; left, composite visible image) and GeMS (right, composite infrared image). Because of the amount of dust, largely opaque to visible light, the views offered by *HST* and by GeMS are significantly different. GeMS's infrared view, at an angular resolution similar or slightly better than *HST* in the visible, provides extremely useful complimentary information to the study of astrophysical objects.

In 2013, Davidge et al. (2013) and Zyuzin et al. (2013) published the first science papers using GeMS data.

7 CONCLUSION

Over 10 yr of efforts and 1 yr of commissioning culminated in 2011 December with the first GeMS/GSAOI science images. This paper is the first paper in a two-part GeMS review. We gave an overview of the history, design and trade-offs, provided a description of the system AITs, and commented on the issues and lessons learned. Paper II reports on GeMS commissioning, performance and operation on sky and GeMS upgrade plans.

In conclusion, *GeMS is fulfilling the promise of wide-field AO*. Over the 85 × 85 arcsec FoV of GSAOI, images with FWHM of 80 mas, with exquisite uniformity, are typically obtained under median seeing conditions. Strehl ratio of 40 per cent in *H* band have been obtained, which we believe are the highest to date with an LGS-based AO system on a large telescope, which are typically limited by focus anisoplanatism at this wavelength.

Finally, GeMS, and the experience acquired from it, is also crucial for the design of the AO systems of the future generation of extremely large telescopes (GMT, TMT and E-ELT).

GeMS/GSAOI is a unique instrument, and will no doubt deliver first class science.

ACKNOWLEDGEMENTS

GeMS was a large instrumentation project. In the course of the last 13 yr, it involved people from many different disciplines. The authors would like to recognize the contribution and thank Claudio Arraya, Rodrigo Carrasco, Felipe Colazo, Fabian Collao, Paul Collins, Herman Diaz, Sarah Diggs, Matt Doolan, Anne Drouin, Michelle Edwards, Vincent Garrel, Fred Gillett, Alejandro Gutierrez, Mark Hunten, Stacy Kang, Matteo Lombini Ariel Lopez, Claudio Marchant, Eduardo Marin, Peter McGregor, Brian Miller, Cristian Moreno, Matt Mountain, Peter Pessev, Rolando Rogers, Jean-René Roy, Andrew Serio, Doug Simons, Chad Trujillo, Cristian Urrutia, Jan van Harmelen, Vicente Vergara, Tomislav Vucina, Peter J. Young and the panel members of the many reviews GeMS went through.

Based on observations obtained at the Gemini Observatory, which is operated by the Association of Universities for Research in Astronomy, Inc., under a cooperative agreement with the NSF on behalf of the Gemini partnership: the National Science Foundation (United States), the National Research Council (Canada), CONICYT (Chile), the Australian Research Council (Australia), Ministério da Ciência, Tecnologia e Inovação (Brazil) and Ministerio de Ciencia, Tecnología e Innovación Productiva (Argentina).

Figure 7. GeMS and *HST* complementarity: different wavelengths, different views but the same resolution.

REFERENCES

Beckers J. M., 1988, in Hulrich M.-H., ed., Very Large Telecopes and Their Instrumentation. ESO, Garching, p. 693

Bec M. et al., 2008a, Proc. SPIE, 7015, 701568

Bec M. et al., 2008b, Proc. SPIE, 7019, 70192C

Boccas M. et al., 2008, Proc. SPIE, 7015, 70150X

Bonaccini D., Rigaut F. J., Glindemann A., Dudziak G., Mariotti J.-M., Paresce F., 1998, Proc. SPIE, 3353, 224

Boyer C., Sebag J., Hunten M. R., Saddlemyer L. K., 2002, Proc. SPIE, 4494, 167

Carrasco E. R. et al., 2012, Proc. SPIE, 8447

Cortés A., Poyneer L., Neichel B., Ammons M., Rudy A., Guesalaga A., 2013, in Esposito S., Clenet Y., Fusco T., Hubin N., Véran J.-P., eds, AO4ELT3, Analysis of the Frozen Flow Assumption using GeMS Telemetry Data, available at: http://ao4elt3.sciencesconf.org/browse/author

d'Orgeville C., McKinnie I., 2003, Laser Guide Star Conventional and Multiconjugate Adaptive Optics at the Gemini Observatory: From One Sodium Laser Beacon to Five. p. 737, doi:10.1109/CLEOE.2003.1313812

d'Orgeville C., Rigaut F. J., Ellerbroek B. L. CLEO/Europe, 2000, Proc. SPIE, 4007, 131

d'Orgeville C., Bauman B. J., Catone J. W., Ellerbroek B. L., Gavel D. T., Buchroeder R. A., 2002, Proc. SPIE, 4494, 302

d'Orgeville C. et al., 2003, Proc. SPIE, 4839, 492

d'Orgeville C. et al., 2008, Proc. SPIE, 7015, 70152P

d'Orgeville C. et al., 2012, Proc. SPIE, 8447

Dalesio L. R. et al., 1994, Nucl. Instrum. Methods Phys. Res. Sect. A, 352, 179

Davidge T., Carrasco E., Winge C., Pessev P., Neichel B., Vidal F., Rigaut F., 2013, PASP, 125, 1181

Dicke R. H., 1975, ApJ, 198, 605

Ellerbroek B. L., 1994, J. Opt. Soc. Am. A, 11, 783

Ellerbroek B. L., 2002, in Vernet E., Ragazzoni R., Esposito S., Hubin N., eds, Beyond Conventional Adaptive Optics. ESO, Garching, p. 377

Ellerbroek B. L., Cochran G., 2002, Proc. SPIE, 4494, 104

Ellerbroek B., Rigaut F., 2000, Nature, 403, 25

Ellerbroek B. L., Rigaut F., 2001, J. Opt. Soc. Am. A, 18, 2539

Ellerbroek B. L. et al., 2003, Proc. SPIE, 4839, 55

Elston R., Raines S. N., Hanna K. T., Hon D. B., Julian J., Horrobin M., Harmer C. F., Epps H. W., 2003, Proc. SPIE, 4841, 1611

Flicker R., 2001, Opt. Lett., 26, 1743

Flicker R., 2003, PhD thesis, Lund University

Flicker R., Rigaut F., 2002, in Vernet E., Ragazzoni R., Esposito S., Hubin N., eds, Beyond Conventional Adaptive Optics. ESO, Garching, p. 377

Flicker R., Rigaut F. J., Ellerbroek B. L., 2000, Proc. SPIE, 4007, 1032

Foy R., Labeyrie A., 1985, A&A, 152, L29

Fried D. L., Belsher J. F., 1994, J. Opt. Soc. Am. A, 11, 277

Fusco T., Blanc A., Nicolle M., Beuzit J.-L., Michau V., Rousset G., Hubin N., 2006, MNRAS, 370, 174

Garcia-Rissmann A., Rigaut F., Bec M., Boccas M., Galvez R., Gausachs G., Gratadour D., Neichel B., 2010, in Clenet Y., Conan J.-M., Fusco T., Rousset G., eds, Proc. First AO4ELT Conference, Adaptive Optics for Extremely Large Telescopes. EDP Sciences, 2010

Gemini M. t., 2001, The Gemini MCAO PDR Report. Gemini Observatory, available at: http://maumae.net/gems/MCAO_PDR_report.pdf

Gratadour D., Rigaut F., 2011, in AO4ELT2, Tomographic Phase Diversity for Phase Retrieval on Wide-Field AO Systems. p. 49, available at: http://ao4elt2.lesia.obspm.fr

Guesalaga A., Neichel B., Rigaut F., Osborn J., Guzman D., 2012, Proc. SPIE, 8447

Guesalaga A., Neichel B., Cortés A., Guzman D., 2013, in AO4ELT3, Performance of Two Turbulence Profilers for a MCAO System Under Strong Dome Seeing Conditions, available at: http://ao4elt3.sciencesconf.org/browse/author

Hankla A. K. et al., 2006, Proc. SPIE, 6272, 62721G

James E., Boyer C., Buchroeder R. A., Ellerbroek B. L., Hunten M. R., 2003, Proc. SPIE, 4839, 67

Johnston D. C., Welsh B. M., 1994, J. Opt. Soc. Am. A, 11, 394

Kolb J., 2006, Proc. SPIE, 6272

Lu J., Neichel B., Rigaut F., 2013, in AO4ELT3, Astrometry with the Gemini Multi-Conjugate Adaptive Optics System, available at: http://ao4elt3.sciencesconf.org/browse/author

Marchetti E. et al., 2003, Proc. SPIE, 4839, 317

Marchetti E. et al., 2008, Proc. SPIE, 7015, 70150F

McGregor P. et al., 2004, Proc. SPIE, 5492, 1033

Neichel B. et al., 2010, Proc. SPIE, 7736

Neichel B., Rigaut F., Guesalaga A., Rodriguez I., Guzman D., 2011a, Conf. Proc. Optical Soc. Am., Applied Industrial Optics: Spectroscopy,

Imaging and Metrology, available at: http://dx.doi.org/10.1364/AOPT.2011.JWA32
Neichel B., Rigaut F., Bec M., Boccas M., Fesquet V., dOrgeville C., Trancho G., 2011b, in AO4ELT2, Sodium Photon Return, Spot Elongation and Fratricide Effect: First On-Sky Results with GeMS. p. 54, available at: http://ao4elt3.sciencesconf.org/browse/author
Neichel B., Parisot A., Petit C., Fusco T., Rigaut F., 2012a, Proc. SPIE, 8447
Neichel B. et al., 2012b, Proc. SPIE, 8447
Neichel B., d'Orgeville C., Callingham J., Rigaut F., Winge C. Trancho G., 2013, MNRAS, 429, 3522
Ragazzoni R., Marchetti E., Valente G., 2000, Nature, 403, 54
Rigaut F., 2002, YAO Adaptive Optics Simulation Package (https://github.com/frigaut/yao)
Rigaut F., d'Orgeville C., 2005, C. R. Phys., 6, 1089
Rigaut F., Roy J.-R., 2001, The Science Case for the Multi-Conjugate Adaptive Optics System on the Gemini South Telescope (http://maumae.net/gems/MCAO-SC-V2.0.2.pdf)
Rigaut F., van Dam M., 2013, in AO4ELT3, Elt AO Simulations on a Laptop with YAO, available at: http://ao4elt3.sciencesconf.org/browse/author
Rigaut F. J., Ellerbroek B. L., Flicker R., 2000, Proc. SPIE, 4007, 1022
Rigaut F., Neichel B., Bec M., Garcia-Rissmann A., 2010a, Proc. SPIE, 7736
Rigaut F., Neichel B., Bec M., Boccas M., Garcia-Rissmann A., Gratadour D., 2010b, in Clenet Y., Conan J.-M., Fusco T., Rousset G., eds, Proc. First AO4ELT Conference, Adaptive Optics for Extremely Large Telescopes. EDP Sciences, 2010
Rigaut F. et al., 2011, in AO4ELT2, GeMS sees star light, available at: http://ao4elt3.sciencesconf.org/browse/author
Rigaut F. et al., 2012, Proc. SPIE, 8447
Robert C., Conan J.-M., Gratadour D., Petit C., Fusco T., 2010, Proc. First AO4ELT Conference, Adaptive Optics for Extremely Large Telescopes. EDP Sciences, 2010
Roddier F., 1999, Adaptive Optics in Astronomy. Cambridge Univ. Press, Cambridge
Rousset G., Fontanella J., Kern P., Gigan P., Rigaut F., 1990, A&A, 230, L29
Summers D., Abrams D. C., Skvarč J., Amico P., Kuntschner H., 2012, Proc. SPIE, 8447, 84474S
Tallon M., Foy R., 1990, A&A, 235, 549
Thomas S., Adkins S., Gavel D., Fusco T., Michau V., 2008, MNRAS, 387, 173
Trancho G., Bec M., Artigau E., d'Orgeville C., Gratadour D., Rigaut F. J., Walls B., 2008, Proc. SPIE, 7016
van Dam M. A., Le Mignant D., Macintosh B. A., 2004, Appl. Opt., 43, 5458
Widenhorn R., Weber-Bargioni A., Blouke M. M., 2010, Opt. Eng., 49, 4401
Wizinowich P., 2012, Proc. SPIE, 8447
Zyuzin D., Shibanov Y., Danilenko A., Mennickent R. E., Zharikov S., 2013, ApJ, 775, 101

This paper has been typeset from a TEX/LATEX file prepared by the author.